Experimental and numerical Study of U-shape Flexural Plate (UFP) dissipators

A. Baird, T. Smith, A. Palermo & S. Pampanin

University of Canterbury, Christchurch, New Zealand

2014 NZSEE Conference

ABSTRACT: One of the major positive outcomes from the Christchurch earthquakes has been the rise in popularity of low damage structures. The design of such structures aims to limit damage to the structural components so the buildings can be immediately occupied following a significant earthquake without the need for major repairs or possible demolition. Instead of the earthquake energy being dissipated by the development of plastic hinge zones in the structural members, the non-linear behaviour is concentrated in replaceable energy dissipators. Such dissipators must be simple to design, cheap to fabricate, flexible in application, robust and replaceable. The U-shape flexural plate (UFP) dissipator is a simple solution that meets all of these requirements. Consequently, its use in low-damage-design structures has been increasing rapidly. However, limited information was available regarding some of the design characteristics of UFPs, notability the initial and post-yield stiffness. These parameters are critical in seismic application in order to determine the dissipative capacity as well as the maximum possible force developed by such a device. A parametric study of the UFP device has been undertaken using a combination of experimental testing and finite element analyses. Based on the data collected, equations which predict the force-displacement behaviour of the dissipator are presented along with preliminary guidelines for their design.

1 INTRODUCTION

The U-shape flexural plate (UFP) is a form of flexural dissipator initially proposed by Kelly et al. (1972) as a means of providing energy dissipation between structural walls. It has had a recent rise in popularity due to its successful application in coupled shear walls, particularly rocking PRESSS (Priestley et al., 1996) or PRES-LAM (Palermo et al., 2005) walls which have also had a recent rise in popularity. UFPs are also cheap to fabricate and exhibit large stable hysteretic behaviour. Although simple design equations have been developed for calculating the yield force of UFPs, the maximum force of a UFP device exceeds the yield force due to strain hardening of the steel. Tests by other researchers have shown that stresses are typically in the order of 145 – 215% that of the yield stress obtained from direct tension tests. (Iqbal et al., 2007; Kelly et al., 1972; Pampanin, 2010). Accurately quantifying this maximum force is critical in order to ensure capacity design principles are upheld and that low-damage hybrid systems will re-centre as intended. Calculation of the initial stiffness is also critical in order to ensure the device will activate during the expected earthquake displacements. If the UFP does not fully activate during an earthquake due to failure to ensure adequate stiffness, the coupled wall system will have a lower moment resistance than intended and consequently higher drifts and more damage will be likely in the structure.

This paper aims to assist in the design of UFPs by presenting design equations based on a parametric study. This parametric study uses a combination of experimental testing and finite element analyses to verify analytically derived design formulae. The non-linear force-displacement behaviour of UFPs is proposed based on the Ramberg-Osgood (Ramberg & Osgood, 1943) function.

2 BACKGROUND

U-Shaped flexural plates (UFPs) are formed from bending a mild steel plate section around a fixed radius to form a ‘U’ shape, as shown in Figure 1. This bending is performed when the plates are hot in

order to prevent stress concentrations being present in the final U shape. When one side of the UFP is subjected to a displacement relative to the opposite side, the semi-circular section rolls along the plate and work is done at the two points where the radius of curvature is changed from straight to curved and vice versa. Thus the yielding point of the plate is moved back and forth along the plate.

Figure 1. Practical building application of UFPs in the Southern Cross Hospital, Christchurch (left) (Pampanin et al., 2011) and the Nelson-Marlborough Institute of Technology Building, Nelson (centre) (Iqbal et al., 2007) and general UFP arrangement (right)

UFPs can be designed for a large range of possible displacements and force levels by varying the plate thickness, width and radius. Since the maximum strain is also directly related to the geometry, the design can also be made such that the UFP can undergo deformations from multiple earthquake events by considering low-cycle fatigue criteria. UFPs have successfully been used in several structural dissipation applications, more recently as a device between coupled timber shear walls, like those shown in Figure 1.

3 UFP DESIGN

The force provided by a UFP was derived analytically by Kelly et al. (1972) by relating the coupling shear of the UFP to the plastic moment, as shown in Figure 2. The plastic moment can be defined by Equation 1 and is defined when the entire region of a rectangular section has surpassed yield. The theoretical maximum force of a UFP can therefore be determined, as shown by Equation 2.

$$M_p = \sigma_y Z_{UFP} = \frac{\sigma_y b_u t_u^2}{4} \tag{1}$$

$$F_p = \frac{2M_p}{D_u} = \frac{\sigma_y b_u t_u^2}{2D_u} \tag{2}$$

The above equations can also be derived for the yield force using the elastic section modulus, S, rather than the plastic section modulus, Z. For a rectangular section, the yield force is 2/3 the plastic force.

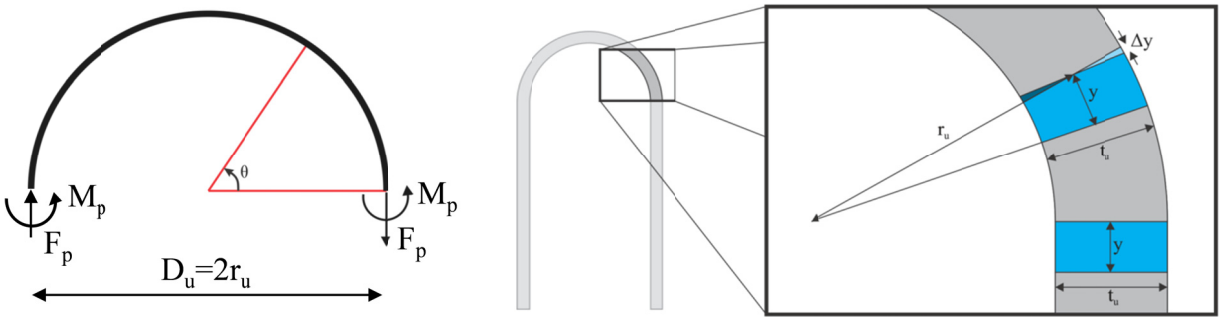

Figure 2. Coupling shear of UFP (left) and derivation of moment in terms of theta (right)

The maximum strain in a UFP can be determined analytically by considering that the maximum deformation of the plate will be in going from straight to curved or vice-versa. Since the radius of the curved section is fixed, it is possible to derive the strain that occurs in the plate from making this transition. Considering a small region of the straight section of the UFP, as illustrated by the square

region in blue in Figure 2 (right), it can be seen that when going from the straight to curved section of the plate, the blue region must deform. Around the outside edge of the UFP the plate must extend by Δy, indicated by the light blue region, and around the inside edge, the plate must compress by Δy, indicated by the dark blue region. Making use of geometry, the maximum strain is therefore equal to the thickness divided by two times the radius, as given by Equation 3.

$$\varepsilon_{\max} = \frac{t_u}{D_u} \tag{3}$$

The yield displacement of a UFP to be determined analytically using energy methods, otherwise known as Castigliano's Second Theorem (Castigliano, 1879). This method finds the deflection from the partial derivative of the strain energy determined by the loads applied. For the UFP we are only considering bending loads since there is no torsional component and the axial deformation will be negligible. The general equation for Castigliano's Theorem is given by Equation 4.

$$\Delta = \frac{\partial U}{\partial F} \tag{4}$$

The strain energy due to bending is found by taking the integral of the moment squared as given in Equation 5.

$$U = \int_0^L \frac{M_y^2(x)}{2EI} \tag{5}$$

The moment due to bending is defined in terms of theta (as shown by Figure 2) by Equation 6.

$$M(\theta) = F_y r_u (1 - \cos\theta) + F_y r_u \tag{6}$$

Solving this gives the yield displacement:

$$\Delta_y = \int_0^L \frac{\partial}{\partial F} \frac{\left[F_y r_u (1-\cos\theta) + F_y r_u\right]^2}{2EI} r_u \partial\theta = \frac{27\pi F_y D_u^3}{16 E b_u t_u^3} \tag{7}$$

The initial stiffness can thus be defined as:

$$k_0 = \frac{F_y}{\Delta_y} = \frac{16 E b_u}{27\pi}\left(\frac{t_u}{D_u}\right)^3 \tag{8}$$

4 EXPERIMENTAL TESTING

In order to characterise the behaviour of the UFPs connections, a series of tests were performed using an Instron Materials Testing Machine. A displacement controlled loading protocol was used to undertake the quasi-static, cyclic loading. The quasi-static loading regime consisted of three cycles at each displacement level, with the maximum displacement being 82.5 mm. The loading rate was varied between 0.5 mm/sec up to 5 mm/sec according to the magnitude of the displacement cycle. The procedure defining the loading protocol was adopted from the ACI recommendations (ACI ITG-5.1, 2007).

4.1 UFP Specimen

One size of UFP was fabricated for testing. Certain aspects of the possible UFP geometry were constrained by the possible materials and machinery available; the plate thickness and width was restricted to the standard metric sizes available; the bend diameter was restricted by the roller sizes available to the fabricator. A local Christchurch company, Bellamy and East Spring Makers, was used to fabricate the UFPs. The largest bend diameter they could provide had an inner diameter of 120 mm. A small ratio between plate thickness and diameter was desired in order to minimise strains and accommodate large displacements. In order to obtain the design force of approximately 10 kN, a plate size of 120 x 8 mm was selected. This gave a yield force of 6.4 kN and a plastic force of 9.6 kN as given by Equation 3. Note the nominal yield strength of an 8 mm plate is 320 MPa (AS/NZS 3678,

1996). A 100 mm straight length between the end of the bend and the bolt fixings was provided to ensure the bend would remain constant. Two 16 mm holes were drilled into the straight region of the plate so the UFP could be bolted into place. Previous testing by Iqbal et al. (2007) made use of welded fixings; however, bolted fixings were chosen due to the desire of the connections to be easily installed and replaceable/removable.

The maximum strain in the plate, as defined by the thickness and diameter of the bend was found to be 6.3%. No failure data exists for UFPs in this region of strain and normalised stroke, so it would be expected that the UFP tested could undergo greater than 150 cycles before failure. Previous tests carried out on UFPs under reversed cyclic loading showed that the mode of failure is characterised by a localised kinking of the plate, followed rapidly by a complete transverse fracture (Iqbal et al., 2007; Kelly et al., 1972).

Two UFPs were tested in parallel in order for the loading to be symmetric. This was done to prevent a moment being applied to the loading apparatus and load cell. The UFPs were tested both by themselves and inside the RHS housing. The testing setup of the UFPs inside the RHS housing is illustrated in Figure 3 (left) and consisted of the two RHS housing being fixed to a base platform with a gap in between. A smaller RHS section (referred to as the loading RHS) was attached to the loading actuator of an Instron testing machine and was driven up and down between the two larger RHS sections in order to impose displacement demand upon the UFPs. A 50 kN load cell was attached to the top of the loading RHS to record the load and a linear potentiometer on the side of the Instron was used to record the vertical displacement.

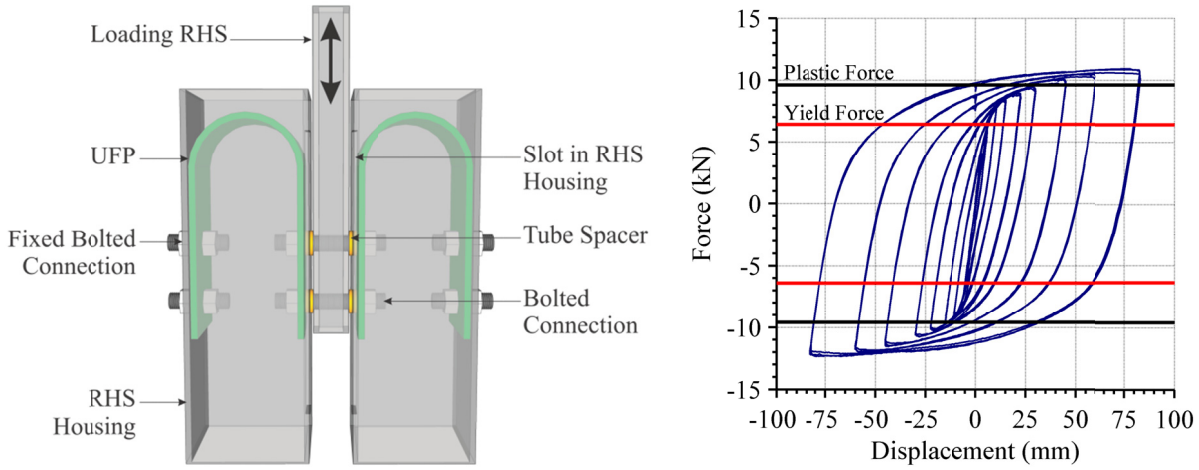

Figure 3. UFP test setup and example of experimental hysteresis loop

The force recorded by the load cell has been halved so the force shown in the force provided by a single UFP. Figure 3 (right) shows the force displacement behaviour of a UFP housed inside the slotted RHS. The definition of the true yield point of a UFP is slightly ambiguous, as the yielding of the UFP results in a gradual change in stiffness; however, it is evident that the analytical plastic force under-predicts the maximum force in the UFP. It can be seen that the maximum force in a single UFP is approximately 12.5 kN. This gives an overstrength factor of approximately 185%. This is in the range suggested by Kelly et al. (1972) who found that overstrength can be in the order of 145 – 215% greater than yield stress obtained from direct tension tests.

The hysteretic behaviour shown in Figure 3 does not suggest failure is imminent since there is no decrease in strength. One of the UFP tests concluded with twenty cycles at maximum stroke and no drop was evident nor was any sign of imminent failure observed.

5 FINITE ELEMENT MODELLING

The ABAQUS finite element programme (ABAQUS Inc., 2011) was used to model the force-displacement behaviour of the UFPs. A Finite Element Model (FEM) of the UFPs tested experimentally was developed and validated against the experimental data.

A 3D deformable solid made up of 2.5 mm tetrahedral mesh elements was used to model the UFPs. The geometry of the model was that of the UFP tested experimentally, a 120 x 8 mm plate with a bend diameter of 120 mm. The steel material was modelled using a plastic isotropic yield model with (combined) cyclic hardening and was based on measured tensile coupon samples of the steel.

Modelling the UFP in the housing required the FEM to be properly constrained; therefore additional boundary conditions were required. This was achieved by using additional rigid body blocks on either side of the UFP. These blocks were assigned the same boundary conditions of the UFP, with one being kept fixed with the fixed side of the UFP, and the other moving vertically with the moving side of the UFP. The interaction between the UFP and the blocks was defined by a surface to surface 'contact interaction'.

The mesh arrangement of the UFP with the block restraints is shown in Figure 4 (top left) The boundary conditions of the UFP with the blocks is shown in Figure 4 (bottom left) along with the contact interaction. The deformed shape of the UFP after the right hand end has been displaced 30 mm downwards is presented in Figure 4 (top and bottom right). The maximum principle stresses are also superimposed onto the deformed shape.

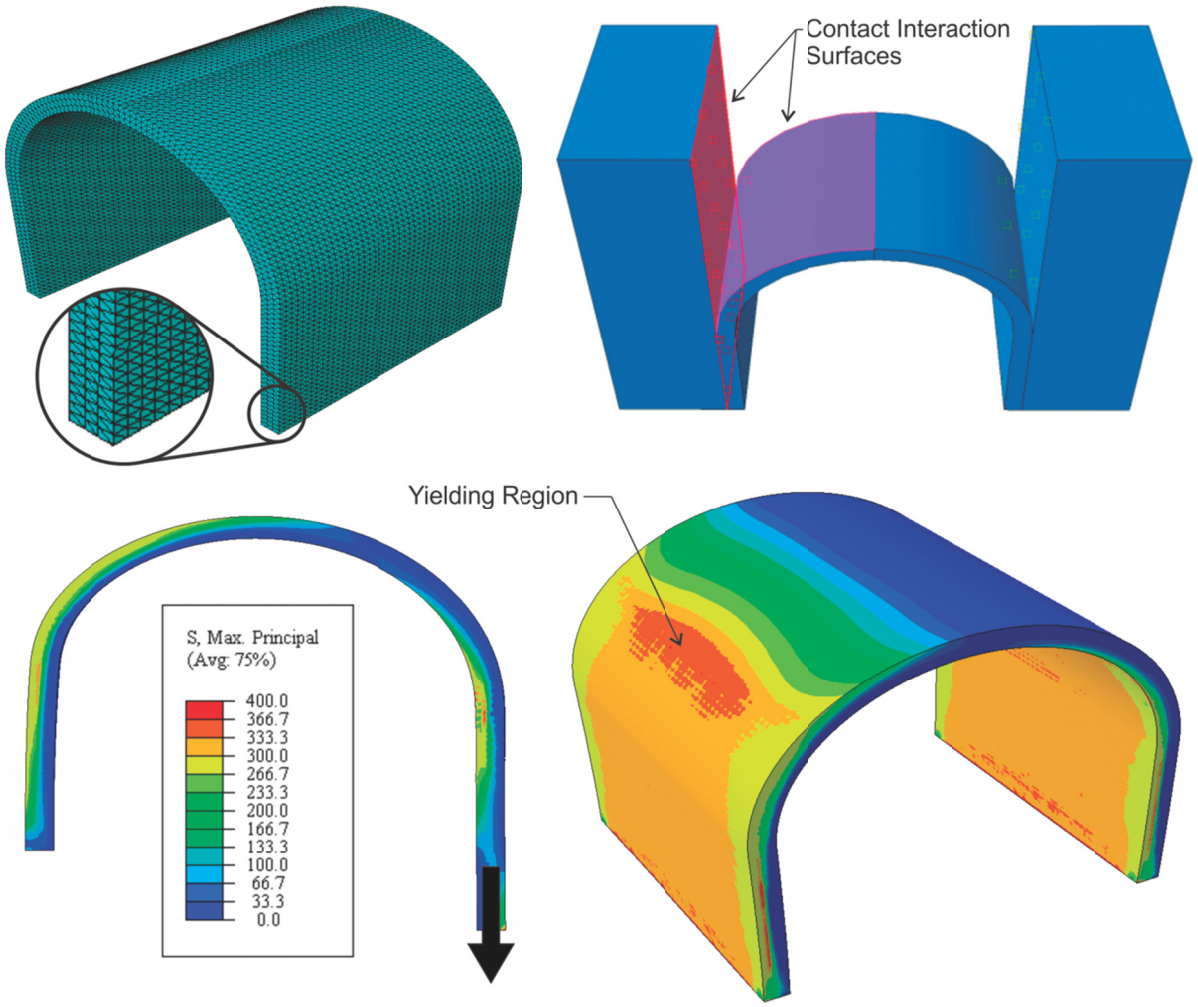

Figure 4. Finite element modelling of UFP: FEM mesh (top left), contact interaction surfaces (top right), principle stresses due to loading (bottom)

The FEM was run using the same displacement cycles as testing however only a single cycle was applied at each displacement level. The elastic material properties of the FEM were based on typical steel properties, with the elastic modulus of the FEM material set at 200 GPa and Poisson's ratio set at 0.3. The yield stress was also set as 320 MPa, the nominal yield stress of an 8 mm hot rolled plate (AS/NZS 3678, 1996). The behaviour of the UFP was calibrated by altering the post-yield plastic material properties. Combined cyclic hardening with a Q-infinity of 120 MPa and Hardening

Parameter of 4.5 was found to best match the experimental post-yielding behaviour.

A contour plot of the stress distribution in the UFP is shown in Figure 4 after being subjected to the cyclic loading. The maximum principle stresses are shown. The contour plot shows how the plate yields in the region where the curvature of the plate changes from straight to curved. It can also be seen how the maximum stresses occur on the outer faces of the plate, analogous to the theory presented in Figure 2.

The numerical force-displacement behaviour of the UFP is shown in Figure 5 (left) along with the experimental behaviour of both UFPs tested (housed and un-housed). The numerical model evidently models the cyclic behaviour of the UFPs very well, capturing the yielding of the plates and the post-yield behaviour very accurately. The maximum force matches the experimental data well but it can be seen in Figure 5 (left) that the FEM did not accurately capture the Bauschinger effect in the steel. Consequently, the numerical hysteresis has a slightly greater area than that of the experimental results. Modelling the non-linear behaviour of steel usually involves some sort of trade-off in accuracy. For this situation, the most important aspect of the modelling was to accurately capture the backbone curve.

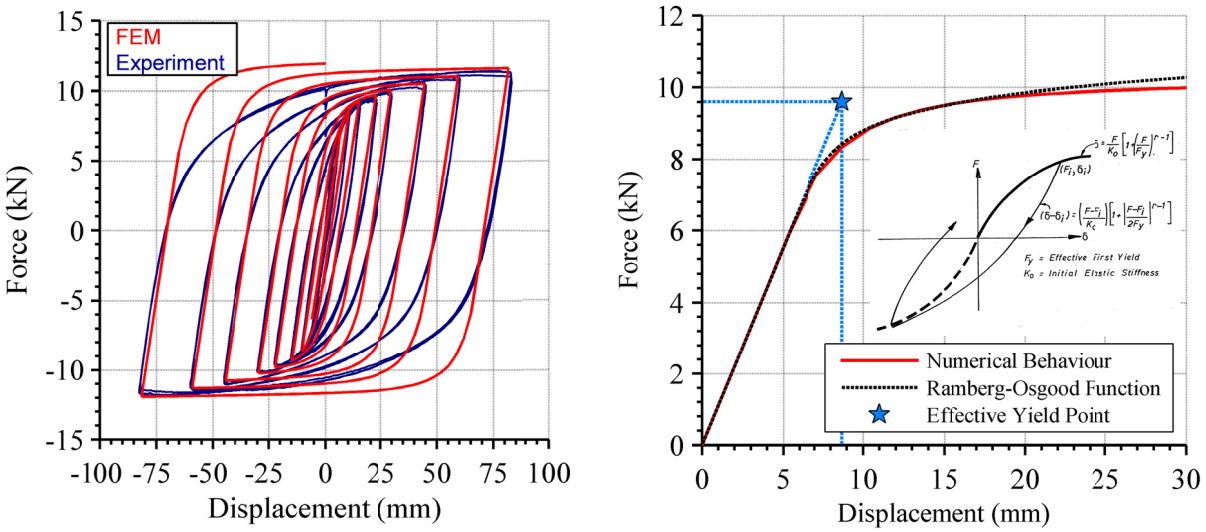

Figure 5. Comparison of FEM hysteresis with experimental results (left), non-linear regression of Ramberg-Osgood function with numerical behaviour (right)

6 PARAMETRIC INVESTIGATION

A parametric investigation of the UFPs has been performed using the FEM developed from the experimental results. The parametric investigation of the UFPs involves varying the plate thickness and bend diameter and examining how these parameters affect the yield force, yield displacement, initial stiffness and R factor. The R factor is a hardening parameter that determines the post-yield stiffness. An R factor of 1 defines a perfectly elastic material and an R factor of infinity a perfectly elasto-plastic material. A Ramberg-Osgood function is fitted to each numerical analysis in order to define the aforementioned parameters. Each numerical analysis consists of a monotonic loading to produce a force-displacement plot similar to that shown in Figure 5 (right). A Ramberg-Osgood R factor of 12 was used to match the data of the UFP tested experimentally.

6.1 Non-Linear Regression

The yield force, initial stiffness, yield displacement and post-yield stiffness of the UFP model have been found from the monotonic response of the finite element analysis (FEA). The decision on whether to determine the UFP parameters based on the monotonic response or the cyclic backbone response is again a trade-off in terms of accuracy and conservatism. The monotonic response underestimates the peak forces attainable by the UFP, and consequently the equivalent displacements predicted are larger for the same force. However, if the cyclic backbone were to be used as the basis of the non-linear behaviour, the peak forces would be overestimated and the equivalent displacements

under-predicted. This is due to the cyclic response relying upon repetitive reverse cycling in order to develop the larger forces attributed to cyclic hardening. It was decided to use the monotonic response for defining the non-linear behaviour since this was deemed the most appropriate for not over-estimating expected forces or underestimating expected displacements.

The non-linear behaviour is approximated with the non-linear Ramberg-Osgood hysteretic rule (Ramberg & Osgood, 1943). The Ramberg-Osgood hysteresis is suited for representing steel behaviour since it shows a smooth elastic-plastic transition. For the Ramberg-Osgood function, the larger the R factor value, the closer the post-yielding behaviour is to being perfectly plastic (Kaldjian & Fan, 1967).

A Ramberg-Osgood function is fitted to the monotonic FEA using a MATLAB regression function that estimates the function coefficients using an iterative least squares estimation (MathWorks Inc., 2011). The initial stiffness can be extracted directly from the numerical data, leaving only the yield force and R factor to require fitting. Figure 5 (right) shows the Ramberg-Osgood function that has been fitted to the numerical data of the monotonic UFP analysis. It can be seen that the Ramberg-Osgood function is an excellent representation of the behaviour. It should be noted that the effective yield point of the Ramberg-Osgood function does not match where a change in stiffness occurs.

6.2 **Parametric Analyses**

The plate thickness of the UFPs was varied based on commercially available metric sizes (5, 6, 8, 10 and 12 mm thick plates). A standard plate width of 100 mm was used. Equation 3 demonstrates that the plate width has a linear relationship with the force in the plate and therefore the results are effectively all per 100 mm of plate width. The inner diameter, D_i, of the UFP was varied from 60 mm to 120 mm in 20 mm increments. The nominal diameter, D_u, is equal to the inside diameter, D_i, plus the plate thickness, t_u. In total, 20 numerical analyses were performed.

The yield force and yield displacement are presented in Figure 6 for the 20 numerical analyses along with the analytical solutions. The results are presented for the various plate sizes and diameters.

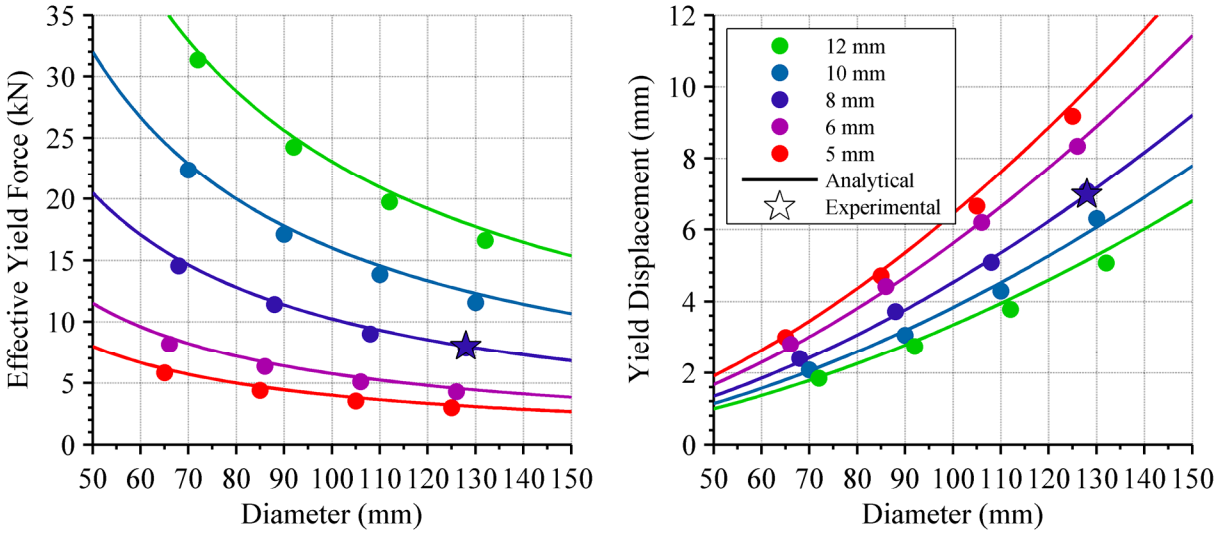

Figure 6. Analytical, numerical and experimental comparison of yield force and yield displacement

The different colours correspond to the five plate sizes considered, with the diameter of the UFP being plotted along the x-axis. The experimental data point has been linearly adjusted to represent a UFP with a plate width of 100 mm instead of 120 mm. The analytical solutions are based on the plastic force, given by Equation 3 and the numerical yield force is defined using the effective yield point as defined by the Ramberg-Osgood function. It can be seen that the analytical plastic force matches the effective yield point of the Ramberg-Osgood function very well.

The analytical solution for the initial stiffness has been found using Equation 8 and is presented in Figure 7 (left) along with the 20 FEM analyses and experimental data point. For simplicity, the data has been presented in non-dimensionalised form. The plate thickness, t_u, has been non-dimensionalised

by the bend diameter, D_u. This dimensionless value is referred to as the 'geometric ratio'. It can be seen that when presented against the geometric ratio, the stiffness data points follow a single curve. The analytical function fits the numerical data points and the single experimental data point extremely well.

An empirical relationship to define the R factor has been proposed that also makes use of the geometric ratio of the UFP. Shown in Figure 7 (right) are the R factors of the numerical analyses plotted against their corresponding geometric ratio. It can be seen that the R factor shows a trend of being larger for greater geometric ratios. This trend appears to flatten out for greater geometric ratios, suggesting a logarithmic function would be a good fit to approximate the data. A logarithmic function is fitted to the data using an iterative approach to minimise the squares of the difference between the function and data points and is shown in Figure 7 (right).

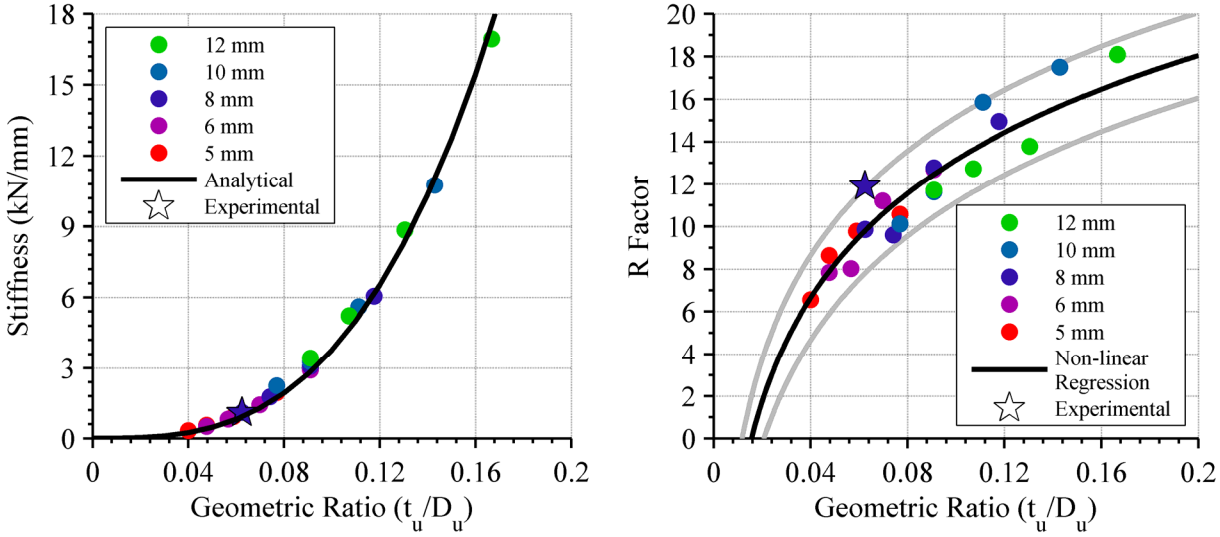

Figure 7. Analytical, numerical and experimental comparison of initial stiffness (left) and non-linear r gression of R factor (right)

The fitted logarithmic function is given by Equation 9. As far as we know, this relationship only relates to the geometries considered here. Also shown in Figure 7 (right) by grey lines are suggested upper and lower bounds for the R factor. These represent a change in the constant presented in Equation 9 from 29.5 to 31.5 and 27.5, respectively.

$$R = 7.1\ell n\left(\frac{t_u}{D_u}\right) + 29.5 \qquad \textbf{(9)}$$

Since the R factor is critical in determining the peak force and peak displacement of the UFP, a thorough design of a UFP may require the use of an upper and lower bound R factor. In this way the maximum probable force provided by the UFP can be established by use of the lower bound R factor. Likewise, the minimum probable force and hence the maximum probable displacement is obtained by use of the upper bound R factor.

6.3 Summary of Recommended Modelling Parameters

Using the combination of experimental, analytical and numerical results, the yield force, initial stiffness and Ramberg-Osgood R factor required for modelling UFP connections are given in Equations 3, 8 and 9 respectively.

$$F_y = \frac{\sigma_y b_u t_u^2}{2D_u} \qquad \textbf{(3)}$$

$$k_0 = \frac{16Eb_u}{27\pi}\left(\frac{t_u}{D_u}\right)^3 \qquad \textbf{(8)}$$

$$R = 7.1\ell n\left(\frac{t_u}{D_u}\right) + 29.5 \quad \textbf{(9)}$$

where

b_u = Width of UFP plate section
t_u = Thickness of UFP plate section
D_u = Diameter of UFP bend
σ_y = Yield stress of UFP
E = Elastic modulus

7 CONCLUSIONS

Formulae for modelling the force-displacement behaviour of UFPs has been derived based on an analytical, numerical and experimental investigation. The analytical formulae, based on fundamental engineering principles, including Castigliano's Theorem, showed a high level of accuracy with the observed experimental and finite element (numerical) results. The post-yield behaviour was found to be well represented by the Ramberg-Osgood function. Using non-linear regression, R-factor values were determined and a function to define the R-factor proposed. Due to scatter of the R-factor values, a lower and upper bound function were also suggested to help ensure a suitable design. Using these tools it is believed a suitably accurate representation of the UFP device can be obtained for use in seismic applications.

REFERENCES

ABAQUS Inc. (2011). Abaqus FEA: Providence, RI., USA.

ACI ITG-5.1. (2007). AAcceptance Criteria for Special Unbonded Post-Tensioned Precast Structural Walls Based on Validation Testing.

AS/NZS 3678. (1996). Structural steel - Hot-rolled plates, floorplates and slabs. Wellington: Standards New Zealand.

Castigliano, C.A. (1879). Théorie de l'équilibre des systèmes élastiques, et ses applications. Turin

Iqbal, A., Pampanin, S., Buchanan, A. H., & Palermo, A. (2007). Improved Seismic Performance of LVL Post-tensioned Walls Coupled with UFP devices. Paper presented at the 8th Pacific Conference on Earthquake Engineering, Singapore.

Kaldjian, M. J., & Fan, W. R. S. (1967). Earthquake Response of a Ramberg-Osgood Structure. Industry Program of the College of Engineering: The University of Michigan.

Kelly, J. M., Skinner, R. I., & Heine, A. J. (1972). Mechanisms of Energy Absorption in Special Devices for use in Earthquake Resistant Structures. Bulletin of the New Zealand Society for Earthquake Engineering, 5(3).

MathWorks Inc. (2011). MATLAB 7.11. Natick, MA., USA.

Palermo, A., Pampanin, S., Buchanan, A., and Newcombe, M. 2005. Seismic Design of Multi-Storey Buildings using Laminated Veneer Lumber (LVL). 2005 New Zealand Society of Earthquake Engineering Conference, Wairaki, New Zealand, pp. 8.

Pampanin, S. (2010). PRESSS Design Handbook. Auckland, New Zealand: New Zealand Concrete Society.

Pampanin, S., Kam W., Haverland, G., Gardiner, S., (2011) "Expectation Meets Reality: Seismic Performance of Post-Tensioned Precast Concrete Southern Cross Endoscopy Building During the 22nd Feb 2011 Christchurch Earthquake" New Zealand Concrete Industry Conference, Rotorua, August

Priestley, M. J. N., Sritharan, S., Conley, J. R., and Pampanin, S. (1999). Preliminary Results and Conclusions from the PRESSS Five-story Precast Concrete Test-Building. PCI Journal, Vol. 44(6), pp. 42-67.

Ramberg, W., & Osgood, W. R. (1943). Description of stress-strain curves by three parameters (Version Technical Note No. 902). Washington, DC.,USA: National Advisory Committee for Aeronatics.